ISA Transactions 166 (2025) 280–297

Contents lists available at ScienceDirect

ISA Transactions

journal homepage: www.elsevier.com/locate/isatrans

Practice article

A data driven fault diagnosis approach for robotic cutting tools in smart manufacturing

Adel Afia [a,b,*], Fawzi Gougam [b], Abdenour Soualhi [c], Mohammed Wadi [d], Mohamed Tahi [a,e], Mohammed Amine Sahraoui [f]

[a] Department of Mechanical Engineering. & Productics, Faculty of Mechanical and Process Engineering, Houari Boumediene University of Science and Technology, Algeria
[b] Department of Mechanical Engineering, Solid Mechanics and Systems Laboratory (LMSS), University Mhamed Bougara Boumerdes, Boumerdes, Algeria
[c] Laboratoire LASPI, University Lyon, UJM-Saint Etienne, Saint-Etienne 42100, France
[d] Electrical & Electronics Engineering Dept, Istanbul Sabahattin Zaim University, Istanbul, Turkey
[e] Laboratory of Advanced Mechanics, University of Science and Technology, Houari Boumediene, Algiers, Algeria
[f] Systems Engineering and Telecommunications Laboratory (LIST), University M'Hamed Bougara Boumerdes, Boumerdes, Algeria

ARTICLE INFO

Keywords:
Manufacturing systems
Fault detection
Model stability
Machine learning
Tool condition monitoring

ABSTRACT

In smart manufacturing within Industry 4.0, tool condition monitoring (TCM) is used to improve productivity and machine availability by leveraging advanced sensors and computational intelligence to prevent tool damage. This paper develops a hybrid methodology using heterogeneous sensor measurements for monitoring robotic cutting tools with four tool states: healthy, surface damage, flake damage and broken tooth. The proposed approach integrates the maximal overlap discrete wavelet packet transform (MODWPT) with health indicators to construct feature matrices for each tool state. Feature selection is performed using the tree growth algorithm (TGA) to reduce computation time and improve feature space separation by selecting only relevant features. The selected features are input into a Gaussian mixture model (GMM) to detect, identify and classify each tool state with high accuracy. The proposed method provides a classification accuracy of 99.04 % for vibration, 95.51 % for torque, and 91.67 % for force signals. Using unseen vibration data, the model achieved a test accuracy of 98.44 %, demonstrating a high degree of generalizability. Comparative analysis demonstrates that our proposed approach provides superior feature discrimination and model stability, balancing computational efficiency and classification accuracy, validating the TGA-GMM framework as an effective solution for tool fault diagnosis in noisy, high-dimensional data.

1. Introduction

Within the fourth industrial revolution, smart manufacturing systems have emerged to improve quality and productivity. Industry 4.0 integrates automated design, machinery, and intelligent monitoring to enhance efficiency and flexibility [1]. However, this evolution has made manufacturing increasingly computerized and complex to monitor, particularly in high-tech systems like robotized multi-axis machining [2].

In all machining equipment, cutting tools must maintain high strength, persistence, and repeatability [3], as product quality depends on tool geometry [4]. However, continuous operation causes tool wear, increases nose radius and affects residual stress [5]. Moreover, undesirable machining conditions may induce tool wear or breakage, influencing surface quality, accuracy, energy consumption, production continuity and costs [4]. Worn tools can suddenly fracture, damaging the machine or spindle [6]. Consequently, tool condition monitoring (TCM) becomes crucial for guaranteeing process stability and ensuring product quality.

Most condition monitoring systems are based on data-driven techniques [7–11], as model-based approaches are neither easily developed nor implemented for complex systems [2]. Data-driven TCM methods, using raw experimental signals, are more suitable for complex systems, including multi-axis robots [12,13]. For instance, Patange et al. [14]

* Corresponding author at: Department of Mechanical Engineering. & Productics, Faculty of Mechanical and Process Engineering, Houari Boumediene University of Science and Technology, Algeria.
E-mail addresses: adel.afia@usthb.edu.dz (A. Afia), f.gougam@univ-boumerdes.dz (F. Gougam), abdenour.soualhi@univ-st-etienne.fr (A. Soualhi), mohammed.wadi@izu.edu.tr (M. Wadi), mohamed.tahi@usthb.edu.dz (M. Tahi), ma.sahraoui@univ-boumerdes.dz (M.A. Sahraoui).

https://doi.org/10.1016/j.isatra.2025.07.021
Received 25 March 2025; Received in revised form 9 July 2025; Accepted 9 July 2025
Available online 12 July 2025

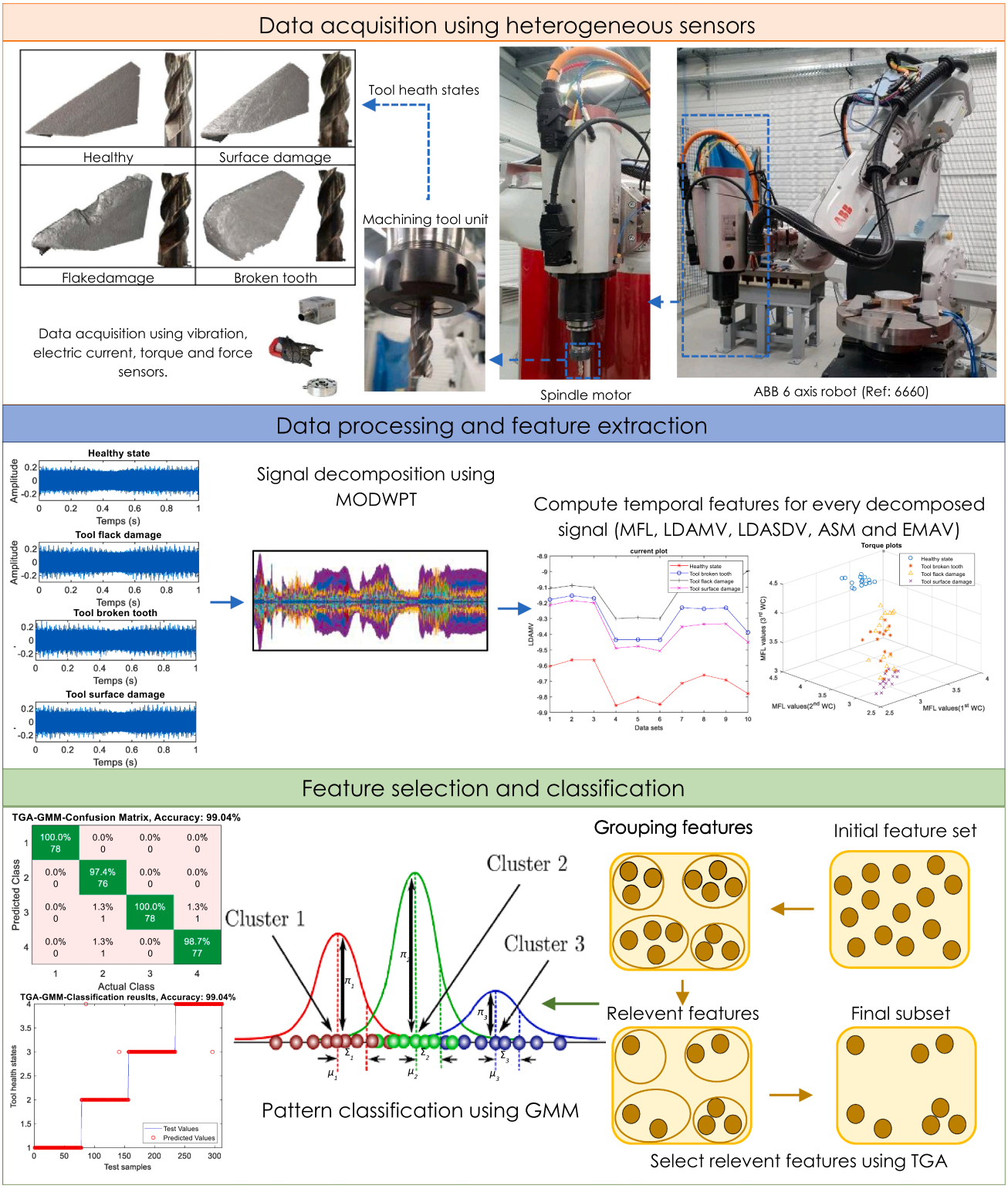

Fig. 1. Intelligent condition monitoring approach framework for smart manufacturing.

analyzed vibration signals from a single-point cutting tool during stainless steel turning to detect defects. Patange and Jegadeeshwaran [15] classified cutting tool conditions in CNC milling via vibration analysis. Similarly, Brito et al. [4] monitored tool wear with vibration signals under unbalanced and variable conditions. Bahador et al. [16] used two accelerometers for tool wear classification in CNC turning, while Aralikatti et al. [17] found that force signals yielded higher accuracy for carbide tool fault diagnosis. Soualhi et al. [2,18] combined multiple sensor data (electric current, vibration, force, torque) for evaluating smart robotic cutting tools. As previously proven, classification models are highly dependent on both data quantity and quality. Variations in machining parameters (feed rate, depth, speed) introduce additional complexity. Considering system diversity and varying conditions, pattern recognition usually requires extensive data covering different machining parameters and failure scenarios. Additionally, sensor data are frequently obscured by noise, complicating fault

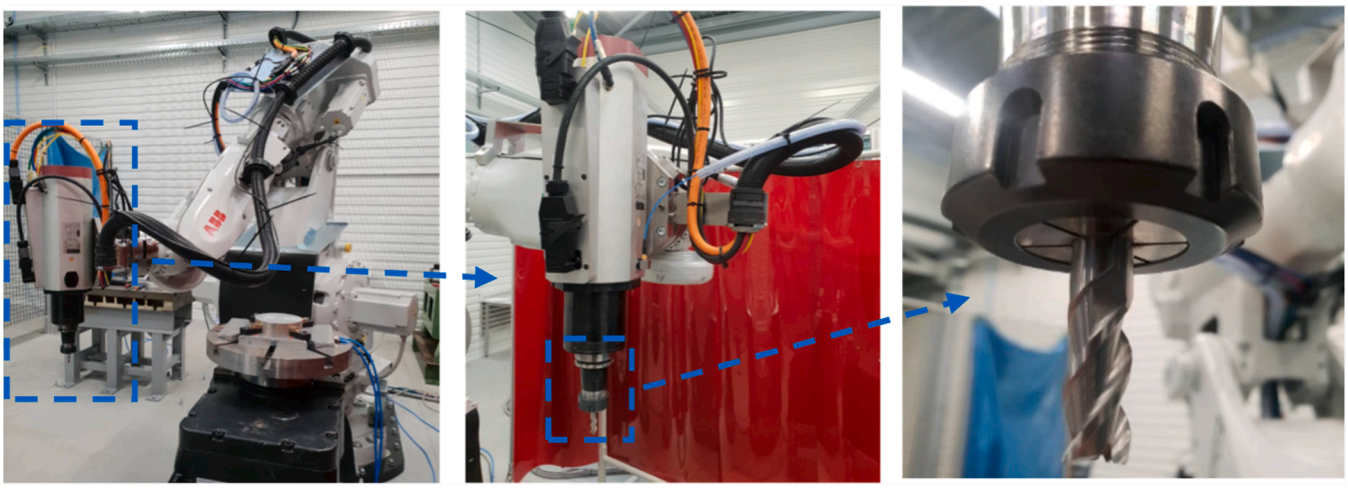

Fig. 2. METALLICADOUR test bench for tool condition monitoring [59].

Table 1
METALLICADOUR test bench spindle motor characteristics [59].

Characteristic parameters	Value
Nominal voltage between phases	380 V
Nominal power output	44 kW
Power supply frequency	50 Hz
Nominal current	22 A
Number of pole pairs (p)	2
Power factor	0.84
Nominal speed	18000 rpm

Table 2
Tool parameters, workpiece, and wear severity levels [59].

Category	Property	Value/ Description
Cutting tool	Diameter	12 mm
	Teeth (Flutes)	3
	Coating	None
	Material	Steel
Workpiece	Material	Aerospace component (ALVEOLUS)
	Shape	Internal cavity
	Application	Aeronautical machining
Wear measurement	Measurement method	3D optical (ALICONA)
	Scale	Micrometer (μm)
	Threshold (VB)	14 μm (Defined by experts)
Defect levels	Level 0	No wear, healthy tool
	Level 1	Surface wear (VB $\geq$ 14 μm)
	Level 2	Flake damage
	Level 3	Broken tooth

detection. Therefore, data must be processed to enhance signal quality and reveal relevant components.

Numerous signal processing techniques have been widely applied to extract useful features from raw data, including empirical mode decomposition (EMD) [19–21], robust EMD (REMD), variational mode decomposition (VMD) and local mean decomposition (LMD) [22–27]. For mechanical fault diagnosis, EMD, for instance, suffers from mode mixing and end effects. Over-shifting occurs when a single frequency component is decomposed into several intrinsic mode functions (IMFs), while under-shifting occurs when several single-component signals are decomposed into a single IMF [28]. This leads to interpretability problems and a reduction in feature quality [28]. Furthermore, selecting the optimal number of sifting iterations within these methods remains a major challenge in the aforementioned methods. For complex systems with large datasets, computational costs must be minimized without compromising decomposition efficiency. Therefore, the maximal overlap discrete wavelet packet transform (MODWPT), which provides uniform frequency bandwidth while avoiding time-varying transformations and allowing original signal reconstruction without loss of useful information, has been widely preferred for condition monitoring [29–35]. MODWPT's ability to provide orthogonal or quasi-orthogonal wavelet bases further enhances feature reliability and classification accuracy [32].

Temporal features, whether dimensional or not, are commonly used to extract statistical characteristics from data, revealing machine status [36,37]. However, since cutting tool data are non-stationary, such features frequently result in erroneous alerts. Therefore, novel health indicators are required to capture signal complexity, structure and, distribution for fault diagnosis. Yet extracted features frequently include redundancies, increasing computations and risking the dimensionality curse. As a result, feature selection for identifying the most relevant features has attracted considerable research attention [38–41]. Feature selection improves prediction accuracy and model generalization by identifying the most relevant features, eliminating redundancy, and reducing dimensionality to prevent overfitting, thus achieving maximum separability in feature space [42]. Since selecting the optimal feature subset from a high-dimensional space is computationally intensive, it is often treated as a combinatorial task, where exhaustive search is impractical [43]. Therefore, Cheraghalipour et al. [44] proposed the tree growth algorithm (TGA), a nature-inspired, population-based metaheuristic that simulates tree growth and competition for resources. TGA has demonstrated strong performance in solving complex engineering problems, outperforming other stochastic optimization methods [45,46].

For feature classification, data-driven models provide a non-linear mapping between features and labels, enabling efficient condition monitoring. Machine learning has advanced fault diagnosis by accurately detecting faulty states. Afia et al. [32] used machine learning to diagnose faults in reciprocating compressors from acoustic signals, while Gougam et al. [47] applied it to classify bearing faults using vibration data from the LASPI test rig [48]. However, most algorithms perform reliably only under stable conditions; variations in load or speed often cause misclassification. For instance, although real-world datasets are commonly obscured by Gaussian-distributed noise and unrelated transients [49], Afia et al. [32] analyzed only steady-state data, without distinguishing between steady-state and transient behaviors. To address such complexity, probabilistic mixture models such as Gaussian mixture models (GMMs) offer flexibility and robustness in representing complex data distributions [50]. In practical applications, GMMs are more efficient in noisy environments than models such as neural networks and support vector machines, due to their lower computational requirements and probabilistic nature [51]. GMMs,

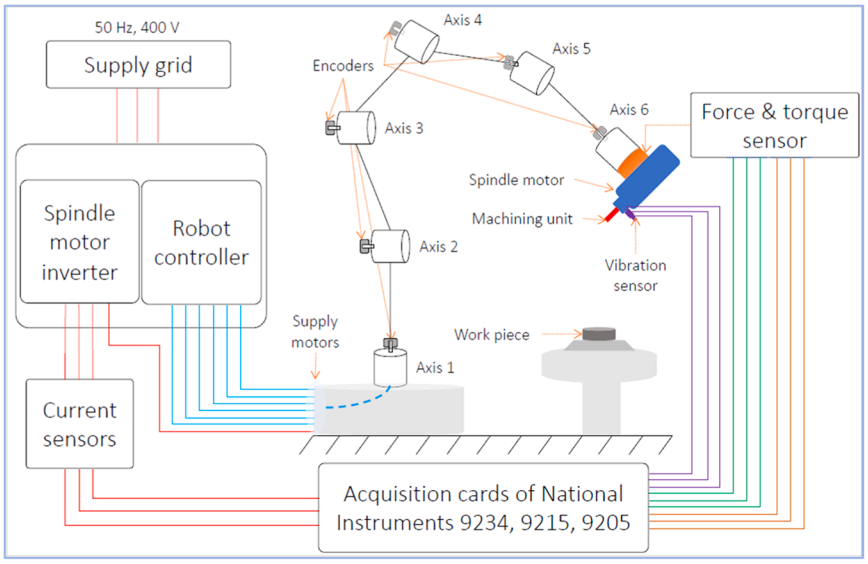

Fig. 3. METALLICADOUR test bench scheme [59].

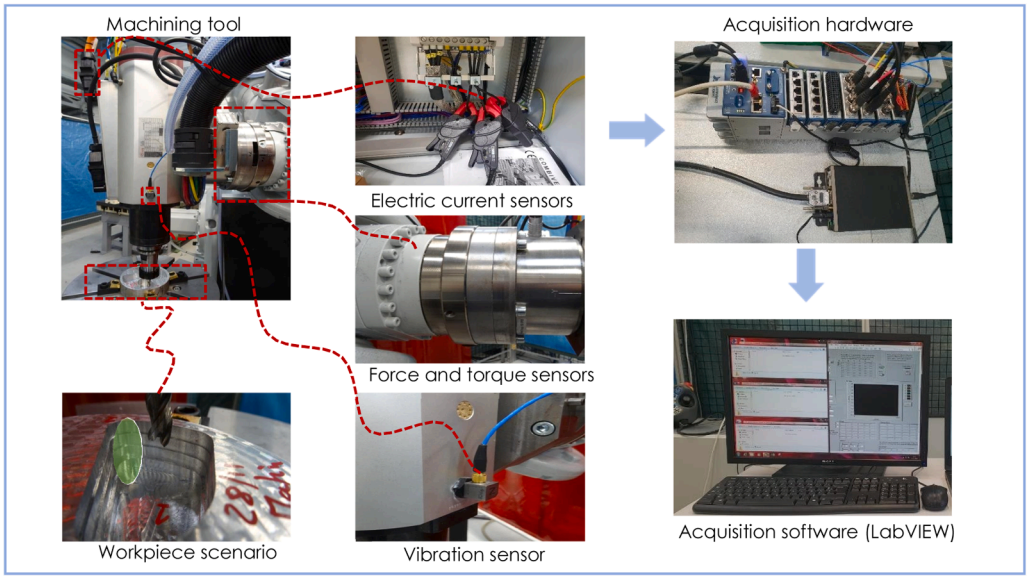

Fig. 4. Data acquisition procedure and sensors placement [18].

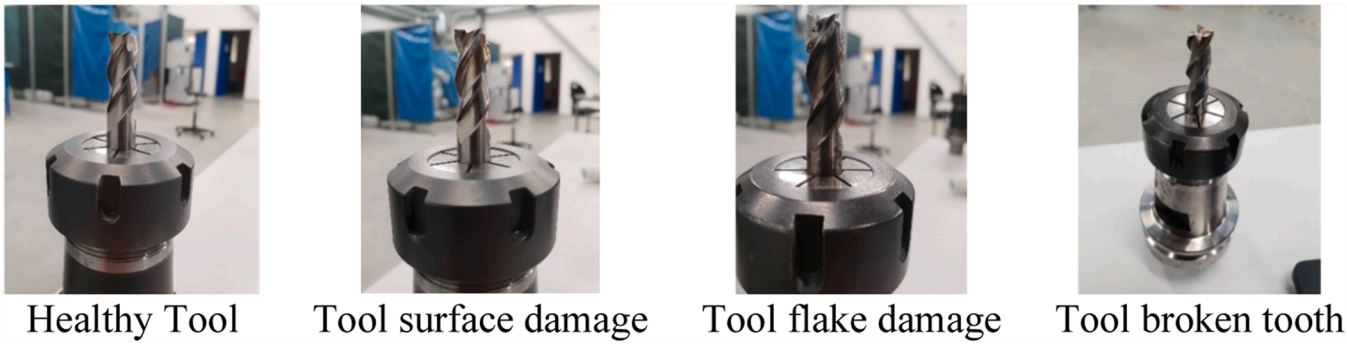

Fig. 5. Illustration of different tool states [59].

based on normal distribution properties, are probably the most widely used probabilistic models, given their ability to accurately model many natural events using a sufficient number of Gaussian distributions [52].

Contrary to distance-based methods, GMMs cluster data by modeling them as probability distributions [53]. As a result, GMMs are particularly well suited to machine condition monitoring by modeling complex

Table 3
An overview of cutting tool experiments [59].

Cutting tool state	Monitoring parameters	Operating conditions			
		Speed (Hz)	Depth (mm)	Feed rate (mm/mn)	Fs (kHz)
Healthy state	Vibration, force, current, torque	233, 300	5, 10	1890, 2730	25.6
Tool surface damage	Vibration, force, current, torque	233, 300	5, 10	1890, 2730	25.6
Tool flake damage	Vibration, force, current, torque	233, 300	5, 10	1890, 2730	25.6
Tool broken tooth	Vibration, force, current, torque	233, 300	5, 10	1890, 2730	25.6

Table 4
Signals per one tool status for different operating conditions [59].

Operating conditions (depth_feed rate_speed)	Signals per axis or phase	Data points per signal	Total signals
5mm_1890mm/mn_14000rpm	8	128,000	24
5mm_1890mm/mn_18000rpm	8	128,000	24
5mm_2730mm/mn_14000rpm	6	128,000	18
10mm_1890mm/mn_14000rpm	4	128,000	12
Total	—	—	78

data distributions using a probabilistic approach, balancing accuracy and computational feasibility [54–58].

From an engineering perspective, the literature reveals a gap in multi-axis robotic cutting tool condition monitoring, which is increasingly relevant in smart factories. In Industry 4.0, these robots offer greater flexibility and integration with cyber-physical systems compared to traditional CNC machines, enabling complex operations with minimal setup. However, this progress requires advanced monitoring strategies. Early tool wear detection is crucial to maintain process stability, extend equipment life, and ensure manufacturing precision. Undetected defects can cause faulty parts, material waste, and poor surface quality, reducing overall efficiency and reliability. This research responds by presenting an integrated approach to advance robotic tool fault diagnosis by developing a pattern recognition methodology for six-axis machining robots using multi-sensor data, vibration, force, electric current, and torque, under varying feed rates, cutting depths, and spindle speeds. The proposed method combines MODWPT with modified statistical indicators for feature extraction, TGA for feature selection, and GMM for classification. Experimentally validated, this comprehensive approach introduces a novel and practical solution for intelligent monitoring under realistic conditions, supporting predictive maintenance in robotic machining. This unique combination of techniques, previously unapplied in robotic tool fault diagnosis, offers both novelty and practical value.

The paper is organized as follows: Section 1 reviews related work and highlights the main contributions. Section 2 presents the proposed methodology and Section 3 details the experimental study, including setup, key steps and the novel automatic fault diagnosis approach with a comparative analysis. Section 4 concludes the study and outlines future research prospects.

2. Proposed methodology

This section describes the proposed methodology's main steps, as illustrated in Fig. 1.

Signals decomposition: Electric current, force, torque and vibration signals are decomposed using MODWPT with six levels into 64 wavelet coefficients (WCs).

Extracting time-domain features for fault detection: Five health indicators are computed for every extracted WC to quantify signal complexity and variability. Each health indicator is calculated for all extracted WCs to build feature matrices for each tool state.

Feature selection using the tree growth algorithm (TGA): To enhance classification accuracy and reduce computational complexity, TGA is applied to the extracted feature matrices. TGA systematically selects the most relevant features while eliminating redundant and less informative ones. By simulating inter-tree competition for resources, TGA optimizes feature selection, improving model generalization and predictive accuracy.

Pattern classification using Gaussian mixture model (GMM): After feature selection, GMM is employed for fault classification. GMM is a probabilistic clustering technique that models the distribution of extracted features as a mixture of multiple Gaussian components.

In contrast to conventional approaches often based on deep learning or manually constructed features, our approach leverages the multi-resolution capabilities of MODWPT to retain crucial time-frequency features, as well an advanced TGA application simulating environmental ecological competition to optimize feature selection. In addition to improving interpretation, this significantly reduces complexity for real-time implementation. GMM enables flexible clustering and quantification of uncertainty in fault classification, making our new fault classification method both robust and scalable.

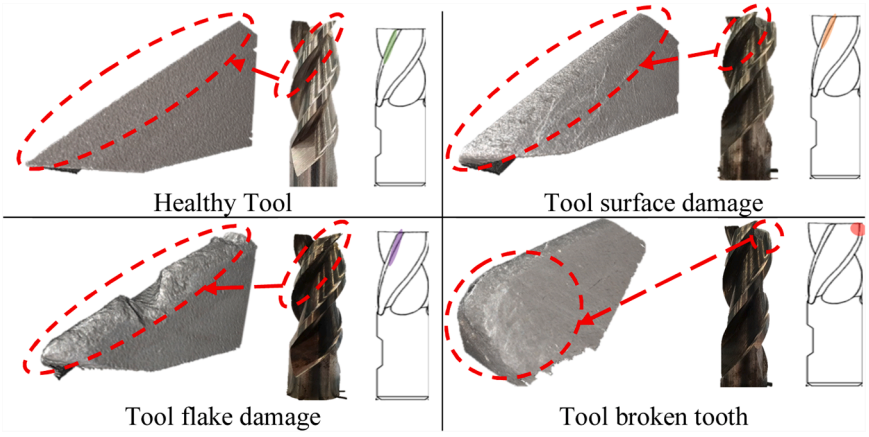

Fig. 6. Tool edge states illustrated in micro scale and schematic views.

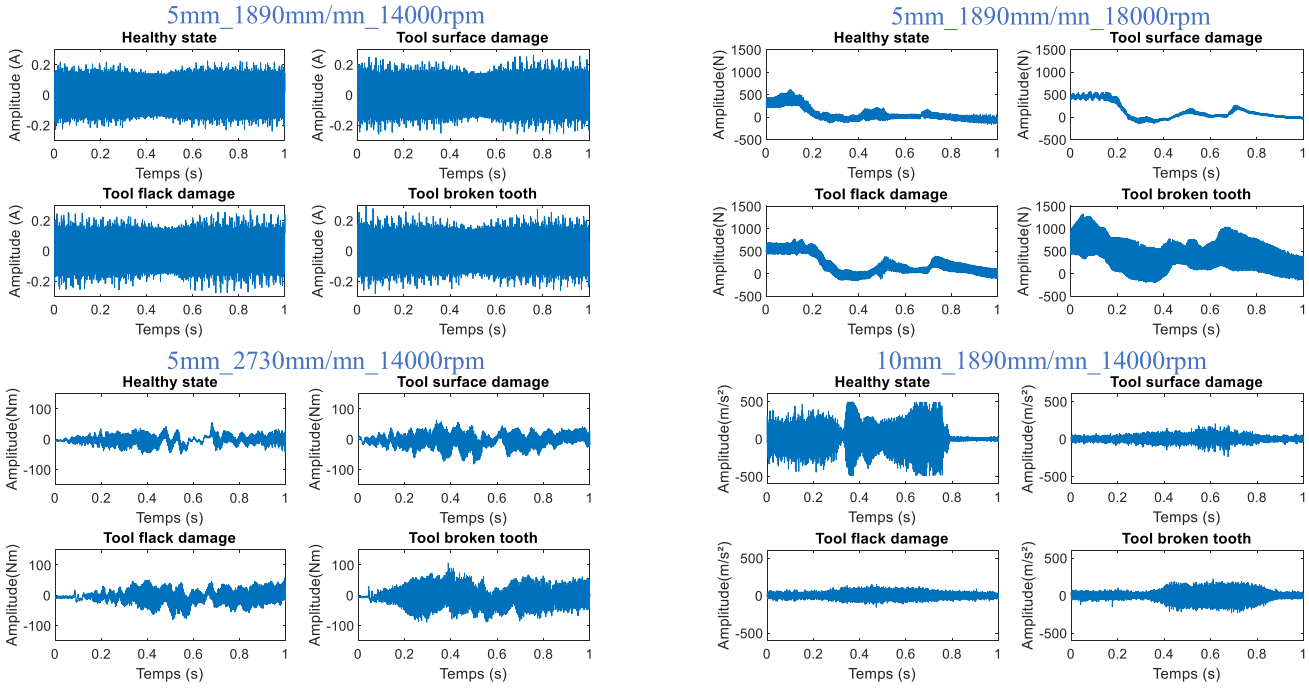

Fig. 8. Time domain signals.

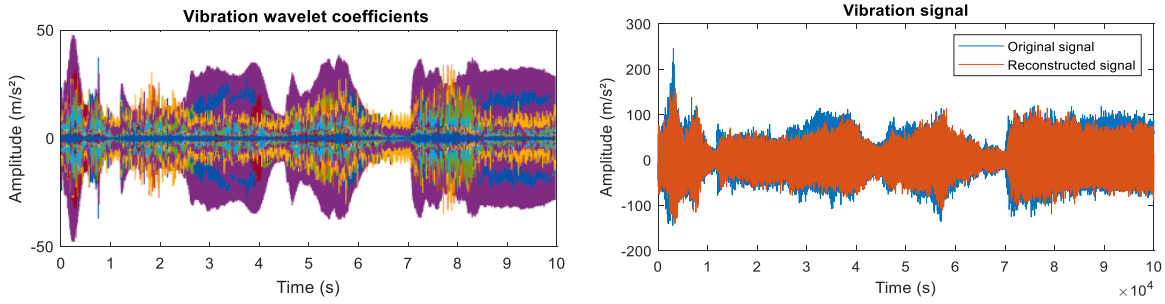

Fig. 9. Wavelet coefficients and reconstructed vibration signal.

3. Condition monitoring for smart manufacturing

3.1. Experimental description

The METALLICADOUR technology transfer center test rig has been considered to monitor a machining tool mounted on a motorized spindle at the end of an ABB 6660 robot axis (see Fig. 2) [59]. This robot is employed for machining aluminum blanks. Each axis is driven by a reciprocating servomotor to ensure precise motion control. The sixth axis, in particular, is equipped with a three-phase motor (specifications in Table 1) that powers a flat-end mill with three cutting edges, commonly used in such machining tasks.

The resulting workpieces are components typically used in aerospace applications. An IRC5 controller powers and coordinates the robot's motion, while an inverter controls the spindle operation. Table 2 shows the cutting tool and workpiece specifications, as well as the predefined wear severity levels.

For data acquisition, three electric current sensors are located at the inverter output, each corresponding to a tool spindle phase. A 3-axis accelerometer is glued to machining spindle flange with thin, high-strength adhesive, positioned closest to the machining unit. In addition, 3-axis force and torque sensors are mounted between the robot's sixth axis and the machining spindle. The sensor data are acquired using National Instruments software (LabVIEW) at a 25.6 kHz sampling frequency. The test bench diagram and sensor placement are illustrated in Figs. 3 and 4, respectively.

A total of 16 experiments were conducted, combining four tool states: healthy, surface damage, flake damage and broken tooth (see Fig. 5), with four distinct operating conditions, which varied in cutting depth, spindle speed and feed rate. Table 3 summarizes the complete experimental setup, highlighting the specific operating conditions for the different tool states.

Table 4 contains detailed information on the signal data samples collected for each tool condition, highlighting the size and structure of the dataset. The number of signal samples is influenced in particular by the operating parameters: higher cutting depth and feed rate reduce the overall machining time, which in turn reduces the sample number since signals are acquired continuously throughout the machining process.

After each machining condition, a 3D optical measurement system called ALICONA was used to reconstruct the tool edge image to evaluate its condition. Fig. 6 shows the tool edge condition using schematic representations and micro-scale images captured by the ALICONA.

3.2. Data processing and feature extraction

Recorded electric current, force, torque, and vibration signals are displayed in Fig. 8, respectively, illustrating the healthy state and the three distinct tool defects under various working conditions.

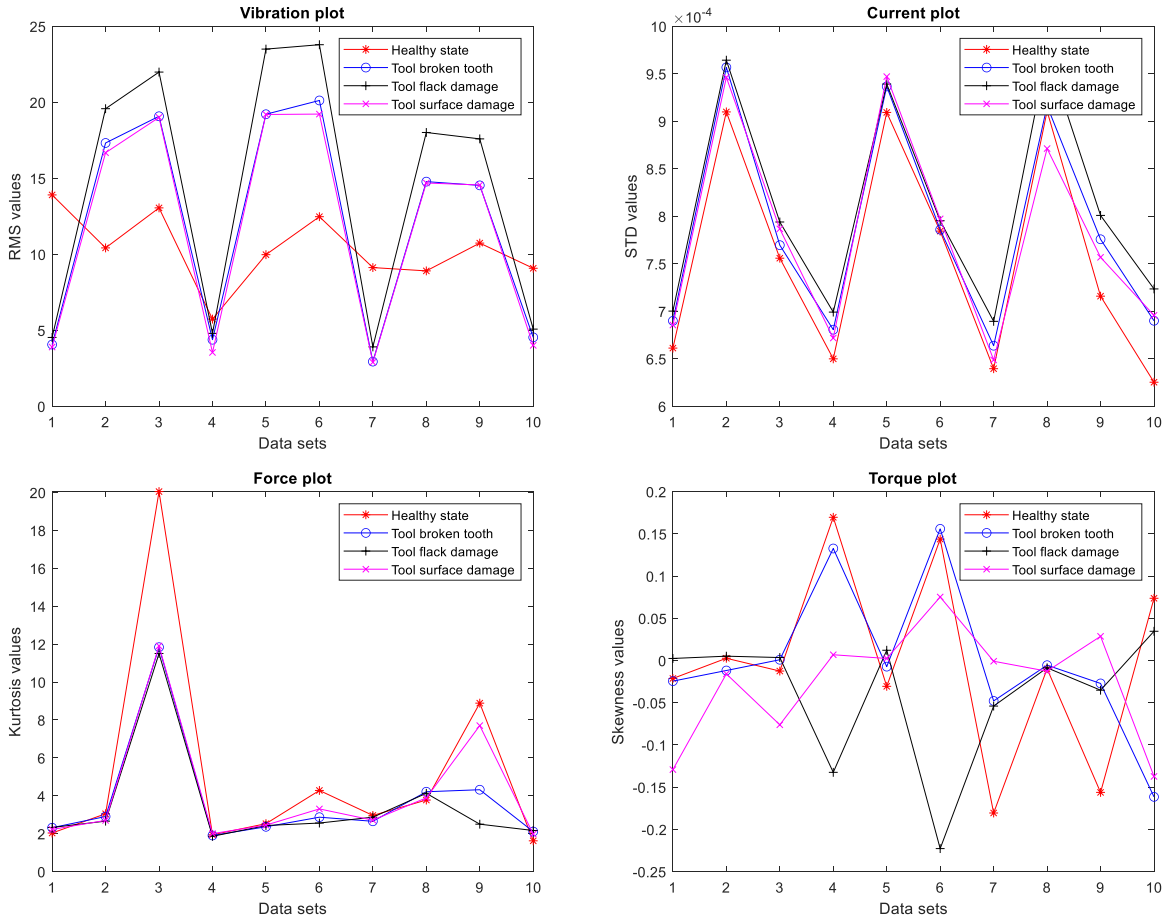

Fig. 10. Conventional health indicators for first ten data measurements.

Despite the varying operating conditions, signals in Fig. 8 almost exhibit a high degree of similarity between different tool states, rendering the visual distinction between healthy and defective tools problematic. The only notable difference is a slight increase in signal time energy in defective tools, though such increases are insignificant for defect identification. Therefore, as highlighted in the introduction, data processing and feature extraction are crucial for fault detection and diagnosis.

3.2.1. Raw data decomposition using MODWPT

Decomposing raw signals provides filtering while preserving critical signal characteristics. Let $x = [x_0, x_1, \ldots, x_{N-1}]^T$ be a discrete-time signal of length N. MODWPT decomposes x into wavelet coefficients $W_{j,n,t}$, calculated using [60]:

$$W_{j,n,t} = \sum_{l=0}^{l-1} \widetilde{f}_{n,l} W_{j-1,\lfloor n/2 \rfloor, \left(t-2^{j-1}l\right) \bmod N} \quad \left(t = 0, \ldots, N-1\right)$$

$$\widetilde{f}_{n,l} = \begin{cases} \widetilde{g}_l \text{ if } n \bmod 4 = 0 \text{ or } 3 \\ \widetilde{h}_l \text{ if } n \bmod 4 = 1 \text{ or } 2 \end{cases}$$

(1)

With j the decomposition level, n the frequency index at level j, and $t = 0,1,\ldots,N\text{-}1$ the time index.

$\widetilde{g}_l$ and $\widetilde{h}_l$ (equation 2) are the rescaled MODWPT low-pass and high-pass filters, respectively, with zeros inserted between the coefficients to preserve temporal accuracy and prevent down-sampling.

$$\widetilde{g}_l = \frac{g_l}{\sqrt{2}} \quad \text{and} \quad \widetilde{h}_l = \frac{h_l}{\sqrt{2}}$$

(2)

In which g_l and h_l are respectively a scaling (low-pass) and a wavelet (high-pass) filter of even length, which are related by [60]:

$$\sum_{l=0}^{L-1} g_l^2 = 1, \sum_{l=0}^{L-1} g_l g_{l+2n} = \sum_{l=-\infty}^{\infty} g_l g_{l+2n} = 0$$

(3)

Both are quadrature mirror filters defined for all non-zero integers n as in:

$$h_l = (-1)^l g_{L-l-1} \quad or \quad g_l = (-1)^{l+1} h_{L-l-1}$$

(4)

Each set of 78 raw signals per tool state, collected from a single sensor (as indicated in Table 4), is decomposed using MODWPT, according to Equation (1), with six levels into 64 wavelet coefficients (WCs). Fig. 9 presents WCs across different frequency bands, obtained from vibration signal for a surface tool defect under operating parameters (5 mm depth, 1890 mm/mn feed rate, and 230 Hz speed), highlighted by different colors, in addition to the filtered reconstructed signal.

3.2.2. Health indicator construction

Time-domain features are important for detecting signal pattern changes, highlighting variations indicative of different machine states by providing valuable insights into machine conditions, with deviations in overall signal energy often signaling faults or anomalies. In this subsection, five health indicators are proposed to be applied to every WC obtained in subsection 3.2.1, where x is the time-domain signal while N is the total number of data points [23]:

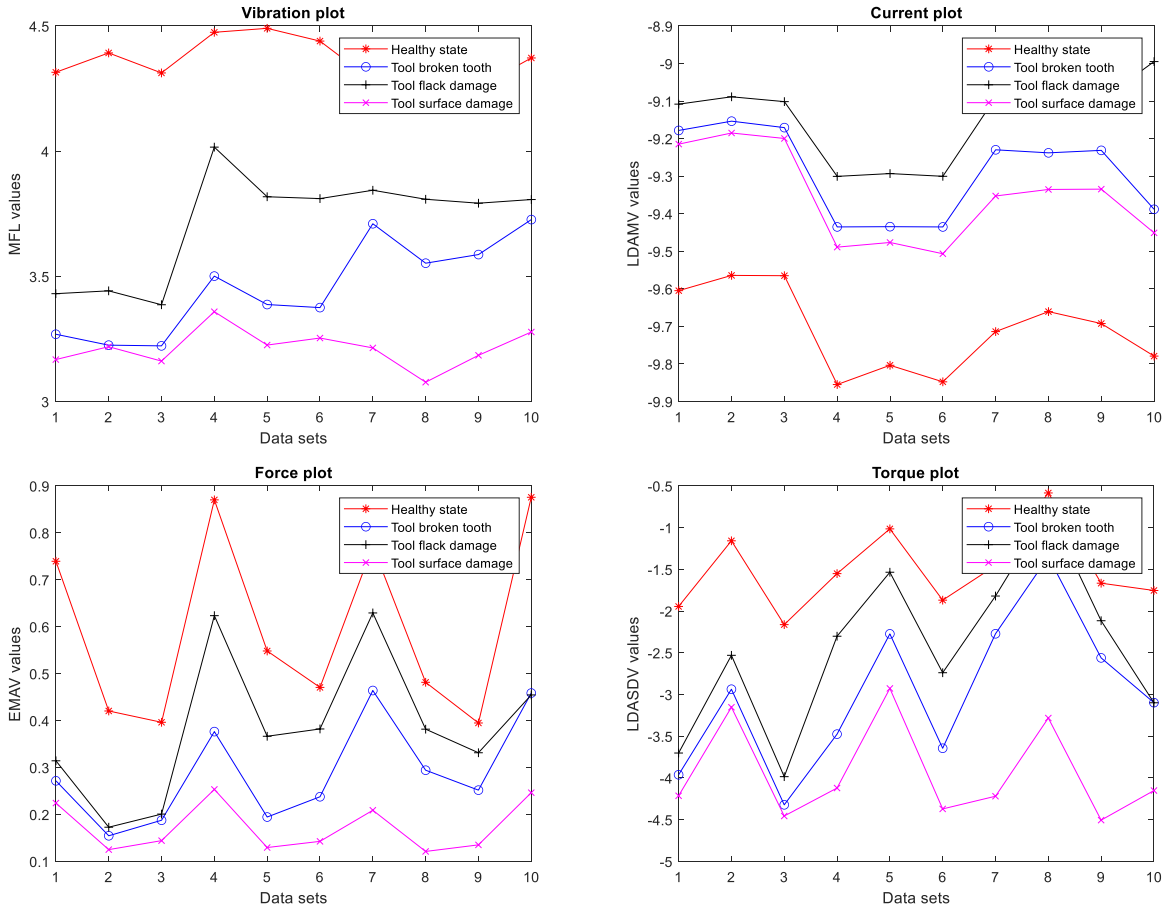

Fig. 11. Proposed health indicators for first ten data measurements.

- **Maximum fractal length (MFL):**

MFL quantifies a signal's fractal complexity by capturing its self-similarity and structural characteristics, and it is defined mathematically in:

$$MFL = \log_{10}\left[\sqrt{\sum_{n=1}^{N-1}[x(n+1)-x(n)]^2}\right] \quad (5)$$

For TCM, a high MFL reflects increased signal irregularity and fragmentation, often associated with abnormal tool induced vibrations. MFL provides a physical link between fractal geometry and mechanical degradation.

- **Log difference absolute mean value (LDAMV):**

LDAMV measures the average magnitude of the first differences between successive data points, providing a consistent measure of signal variability. It is given by:

$$LDAMV = \log\left[\frac{\sum_{t=1}^{N-1}|x(t+1)-x(t)|}{N}\right] \quad (6)$$

Physically, LDAMV captures subtle fluctuations in cutting force or vibration signals, which often increase with tool wear or defects, reflecting instability and uneven load transmission at the tool/workpiece interface.

- **Log difference absolute standard deviation value (LDASDV):**

LDASDV provides a measure of signal variability by evaluating the standard deviation of the first differences between successive data points. It is calculated by:

$$LDASDV = \log\left[\frac{\sqrt{\sum_{t=1}^{N-1}[x(t+1)-x(t)]^2}}{N-1}\right] \quad (7)$$

LDASDV reflects the dynamic signal dispersion, which increases in response to intermittent tool chipping, micro cracking or other mechanical inconsistencies. LDASDV provides an indication of the evolving instability of tool dynamics.

- **Absolute value of the summation of exponential root (ASM):**

ASM assesses the signal's distribution and weighted characteristics, offering a nuanced measure of its complexity, and it is defined in:

$$ASM = \left|\frac{\sum_{n=1}^{N}(x(n))^{\exp}}{N}\right|$$

$$\begin{array}{l} if \quad 0.75\times N \geq n \geq 0.25\times N \rightarrow exp = 0.5 \\ elseif \quad \rightarrow exp = 0.75 \end{array}$$

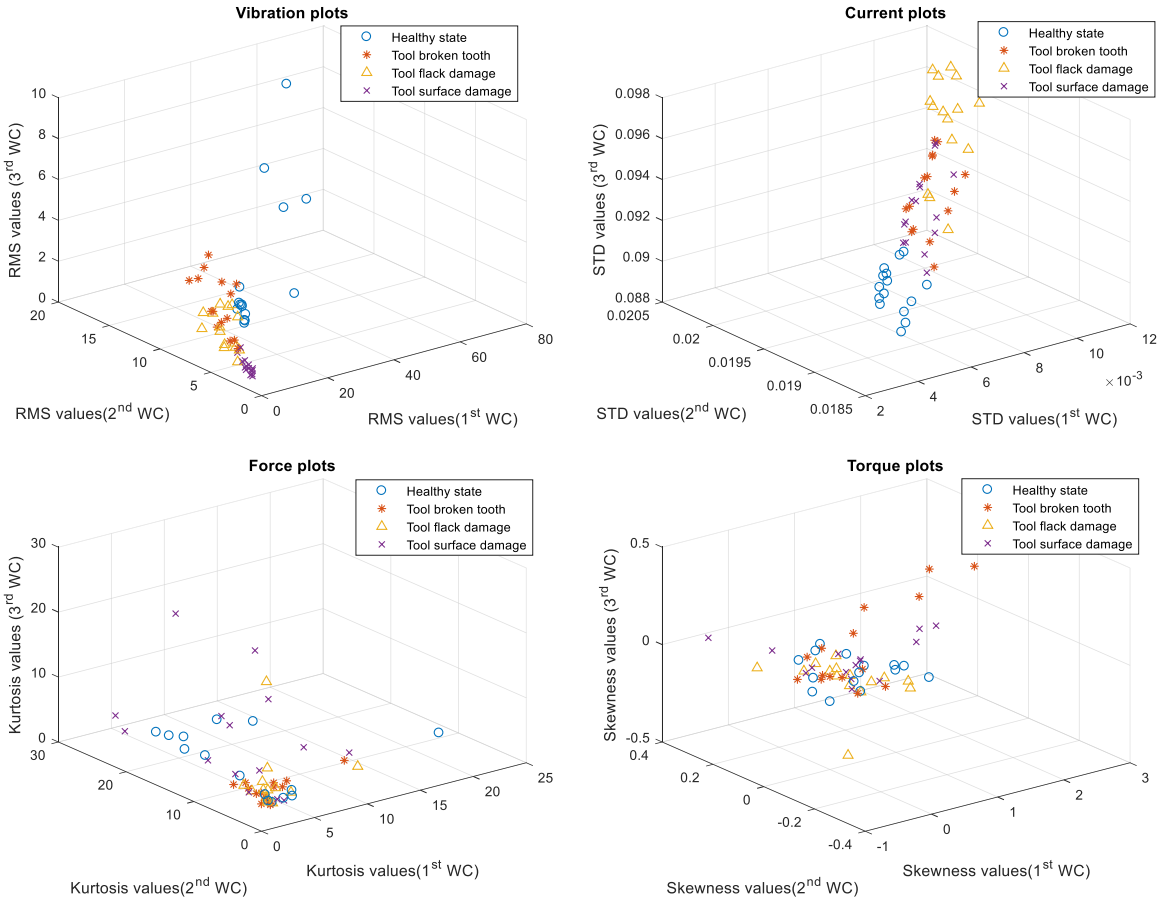

Fig. 12. Conventional health indicators results illustrated in three-dimensional space.

(8)

ASM captures transient behavior and high-impact energy pulses in cutting force and vibration signals, which often correspond to sudden degradation events or impact anomalies, such as tool breakage or the presence of hard material cavities.

- **Enhanced mean absolute value (EMAV):**

EMAV evaluates the signal's average magnitude with varying sensitivity based on the data point's position within the signal. EMAV integrates the magnitude of data points and their position in the signal, providing a differentiated measure of signal characteristics. It is calculated by:

$$EMAV = \frac{\left| \sum_{i=1}^{L} (x(i))^p \right|}{N}$$

$$\begin{aligned} &if \quad 0.8 \times N \geq n \geq 0.2 \times N \rightarrow p = 0.75 \\ &elseif \quad \rightarrow p = 0.5 \end{aligned}$$

(9)

EMAV focuses on localized changes over time, enabling tool wear progression and time-varying signal trends to be detected. This feature improves response to early degradation patterns in sequential sensor readings.

As cutting tool data are non-stationary, the proposed health indicators are designed to quantify signal complexity and variability, offer insight into its structural characteristics, and evaluate the signal distribution while reducing noise and retaining the main signal information, which is crucial for cutting tool fault detection and classification.

These indicators are used to construct feature matrices representing the respective tool states. For each tool state and each health indicator, a 78×64 matrix is obtained, where 78 represents the number of samples (as indicated in Table 4), and 64 corresponds to the number of WCs. A comparative study between the proposed and conventional indicators, such as root mean square (RMS), standard deviation (STD), kurtosis and skewness, is included. Figs. 10 and 11 illustrate the conventional and proposed health indicators after feature extraction for the first 10 signals for each sensor measurement, respectively.

Contrary to conventional indicators as shown in Fig. 10, Fig. 11 demonstrates that our feature extractor prevents any overlap between the four tool states, regardless of whether sensor measurement is involved. Experimental results validate that our feature extractor can robustly differentiate and classify various tool states, ensuring almost perfect separation between healthy and failure states.

An additional comparative study between the proposed and conventional indicators is provided. Figs. 12 and 13 show a 3D representation of the values extracted using the conventional and proposed health indicators, respectively, for the first 15 WCs obtained from different sensor measurements.

Based on Figs. 12 and 13, implementing the proposed health indicators, compared to conventional, yields promising results in feature separation, particularly for the vibration data, which exhibits minimal dispersion. However, despite the satisfactory separability of some tool states in most plots, there is a noticeable overlap between some health indicators, especially in the force and electric current plots, where the states of different tool conditions (broken tooth, tool flake damage, and surface damage) are less clearly defined.

The 3D overlap suggests that machine learning models based on spatial distance measures, such as K-nearest neighbors (KNNs), may have difficulties in accurately classifying cutting tool conditions. The confusion between health indicators confirms the high complexity of cutting tool defect detection and classification.

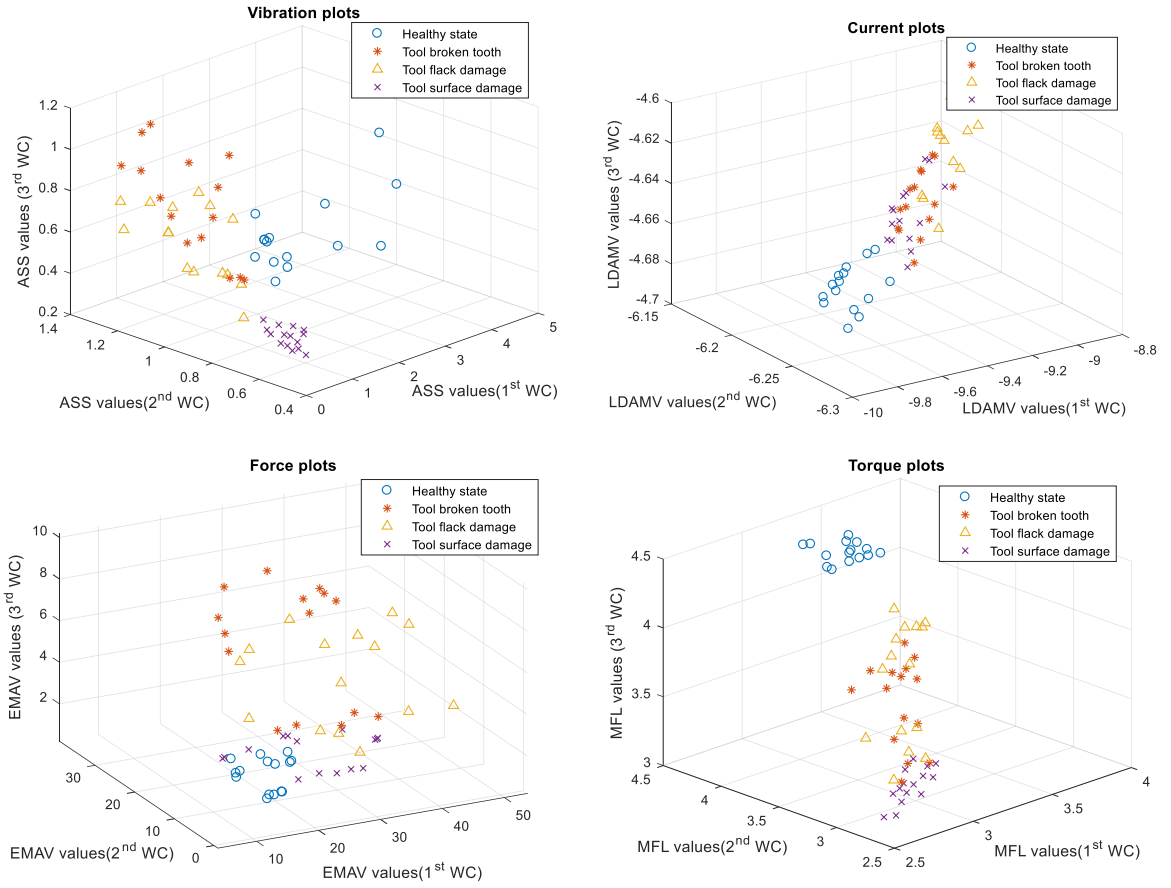

Fig. 13. Proposed health indicators results illustrated in three-dimensional space.

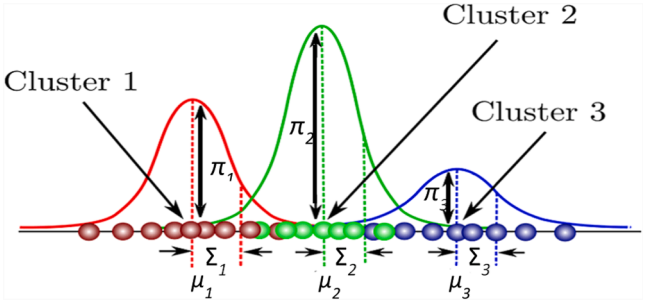

Fig. 14. GMM parameters illustration for 3 clusters.

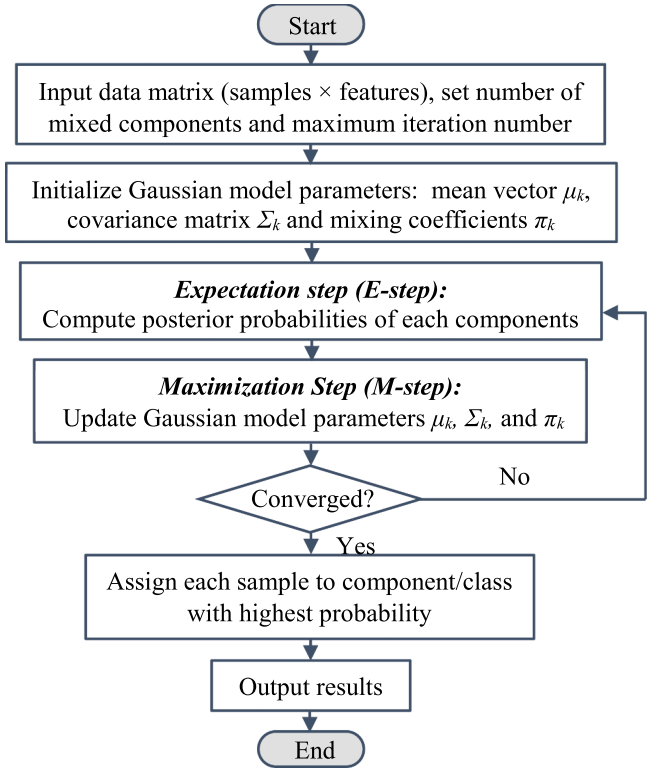

Fig. 15. GMM flowchart.

3.3. Pattern classification

3.3.1. Gaussian mixture model (GMM)

GMMs are probabilistic data clustering techniques assuming the data points originate from a mixture of finite Gaussian distributions with unknown parameters [53]. GMMs are suitable for fault classification in various engineering applications due to their ability to model complex data distributions using a probabilistic approach [50], estimating density functions using expectation maximization (EM) [54,55]. Unlike distance-based methods, GMM are well suited to high-dimensional data, modeling distributions as weighted sums of Gaussian density functions [56]. Although, complex models like SVMs can handle diverse data, they require significant computation [51], whereas GMMs offer efficient solutions for complex, high-dimensional data.

For D-dimensional input $x \in R^d$, GMM assumes K component, each a Gaussian with mean μ_k and covariance Σ_k. The probability density function for k-th Gaussian component is given by [61]:

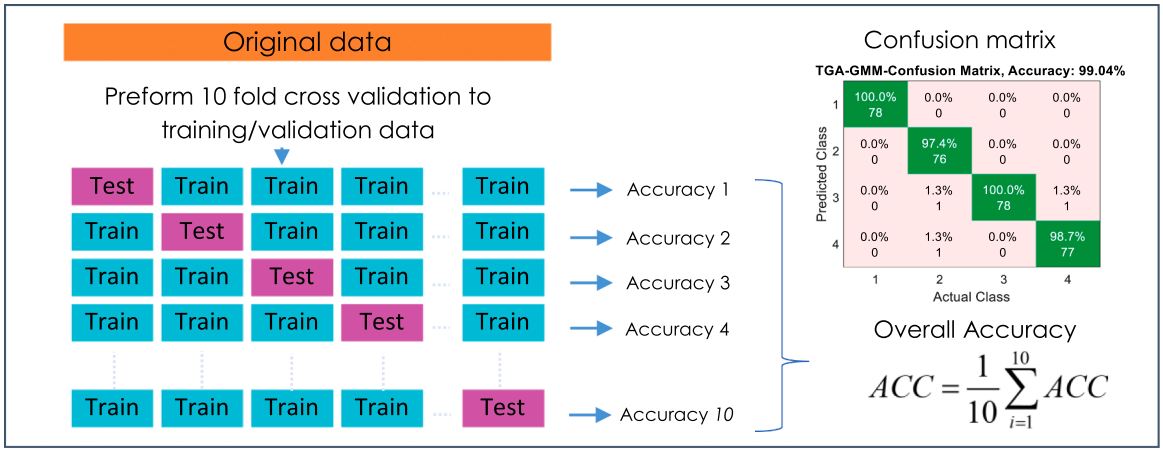

Fig. 16. K-fold cross-validation method.

$$p(x|\mu_k, \sum_k) = \frac{1}{(2\pi)^{D/2}|\sum_k|^{1/2}} e^{(-\frac{1}{2}(x-\mu_k)^T \sum_k^{-1}(x-\mu_k))} \quad (10)$$

π_k is the mixing coefficient corresponding to the *k-th* component, with $0 \leq \pi_k \leq 1$ and $\sum_{k=1}^{K} \pi_k = 1$ constraints. The overall mixture model is expressed as:

$$p(x) = \sum_{k=1}^{K} \pi_k p(x|\mu_k \sum_k) \quad (11)$$

A *K*-dimensional binary random variable *z* is used, with $z_k = 1$ for selected component and 0 otherwise. The marginal distribution of *x* is given as a function of *z* and mixing coefficients *πk*.

A data matrix $X \epsilon R^{N \times D}$, where *N* and *D* are the instance and feature numbers, respectively. The *n-th* row of this matrix is labelled x_n^T. Assuming the instances are independently sampled from the distribution, the log-likelihood function is computed as:

$$\log L(\Theta) = \sum_{n=1}^{N} \log(\sum_{k=1}^{K} \pi_k p(x|\mu_k \sum_k)) \quad (12)$$

where $\Theta = \{\mu_k, \Sigma_k, \pi_k; \quad k = 1,\ldots,K\}$ represents the set of all parameters to be estimated.

GMM's objective is to maximize this likelihood function regarding the parameters μ_k, Σ_k and π_k. This is achieved using the EM algorithm, which iteratively estimates the parameters [61]. Fig. 14 graphically illustrates GMM parameters, while Fig. 15 provides GMM flowchart.

Based on the results in subsection 3.2.2, GMM classifier is expected to provide improved classification accuracy, particularly for overlapping force and torque features. Unlike KNN, based on spatial distance, GMM models the data as a mixture of Gaussian distributions and assigns class probabilities based on likelihood. Consequently, GMM is more efficient at dealing with overlapping data by considering the data's variance and covariance.

3.3.2. Tool fault classification using GMM

The extracted feature matrices in Subsection 3.2.2 using the proposed feature extractor are used to classify tool states with GMM, and are compared with discriminant analysis (DA), multi-class SVM (MSVM), ensemble tree (ET), random forest (RF), and K-nearest neighbors (KNN). This comparative study highlights GMM's advantage in modeling complex, overlapping data distributions through a probabilistic approach. To reduce overfitting, a 10-fold cross-validation is used, in which the dataset (78 samples per condition, as shown in Table 4) is divided into 10 complementary subsets. At each iteration, one subset is retained as a test set to evaluate the model trained on the remaining nine subsets (See Fig. 16). The final classification accuracy is the average accuracy for the 10 models trained across the 10 iterations. The cross-validation method effectively reduces the randomness associated with dataset selection and provides a reliable, scientific assessment of classification model performance.

Fig. 17 shows the average classification accuracy results obtained using various classifiers for each proposed health indicator, compared with the four conventional indicators presented in Subsection 3.2.2 regardless of operating parameters.

According to Fig. 17, using proposed health indicators, GMM consistently achieves high classification accuracy, with 94.87 % for vibration, 94.23 % for torque and 91.35 % for force signals. However, electric current features show significantly lower classification for all models, with a highest accuracy of only 51.64 %. This gap is mainly due to the fact that electric current signals are influenced by various external factors such as motor load fluctuations and power supply variations, rendering them less effective at detecting localized tool faults. By contrast, vibration, force and torque signals are more directly sensitive to tool wear and cutting resistance, enabling more accurate classification. DA achieves good classification results, often exceeding 90 % accuracy, indicating its reliability for various fault indicators. MSVM, RF and ET, despite their ability to handle various data distributions, offer lower accuracy in many cases. These models require substantial computing resources for training and prediction, making them less effective for real-time applications than GMM. GMM captures non-linear patterns and complex data structures more naturally than MSVM, RF or ET, which rely on distinct separations or decision boundaries that might not fit overlapping cases properly. Moreover, GMM is less sensitive to noise in overlapping regions than RF and ET, as it incorporates noise into the probabilistic distribution of the data rather than imposing strict limits, thereby reducing classification errors. KNN, meanwhile, performs poorly due to its dependence on spatial distance, which proves inadequate when dealing with overlapping features.

To conclude, this comparative study demonstrates that combining MODWPT, the proposed indicators, and GMM is efficient approach for accurate fault classification in manufacturing systems. GMM's probabilistic nature ensures optimal performance, making it a superior choice for handling complex and overlapping data distributions in tool condition monitoring.

3.4. Feature selection

3.4.1. Tree growth algorithm (TGA)

TGA, developed by Cheraghalipour and Hajiaghaei-Keshteli [44], is an innovative metaheuristic algorithm inspired by tree competition for nutrients and light. TGA exceeded many state-of-the-art stochastic optimization methods through benchmark tests on engineering tasks [62]. In TGA, an iteration is divided to four phases based on fitness

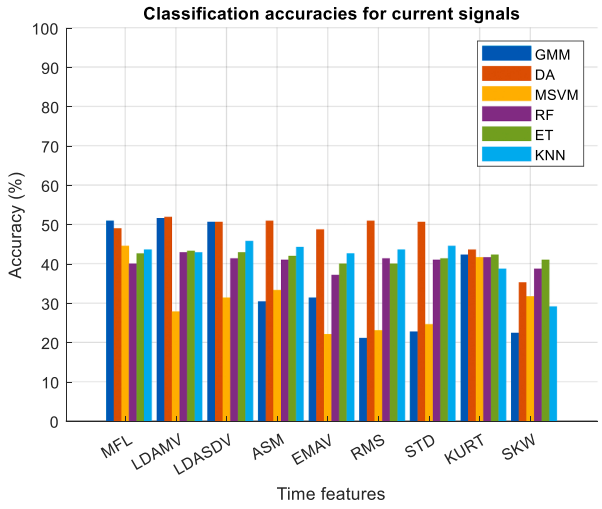

Indicators	GMM	DA	MSVM	RF	ET	KNN
MFL	50.96%	49.04%	44.55%	40.06%	42.63%	43.59%
LDAMV	51.60%	51.92%	27.88%	42.95%	43.27%	42.95%
LDASDV	50.64%	50.64%	31.41%	41.35%	42.95%	45.83%
ASM	30.45%	50.96%	33.33%	41.03%	41.99%	44.23%
EMAV	31.41%	48.72%	22.12%	37.18%	40.06%	42.63%
RMS	21.15%	50.96%	23.08%	41.35%	40.06%	43.59%
STD	22.76%	50.64%	24.68%	41.03%	41.35%	44.55%
Kurt	42.31%	43.59%	41.67%	41.67%	42.31%	38.78%
SKW	22.44%	35.26%	31.73%	38.78%	41.03%	29.17%

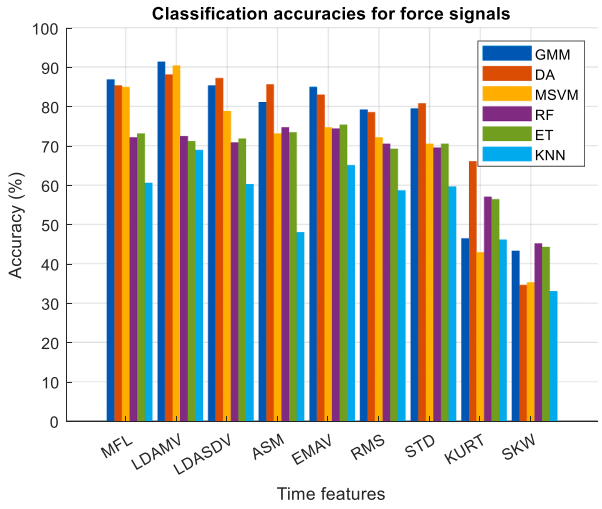

Indicators	GMM	DA	MSVM	RF	ET	KNN
MFL	86.86%	85.26%	84.94%	72.12%	73.08%	60.58%
LDAMV	91.35%	88.14%	90.38%	72.44%	71.15%	68.91%
LDASDV	85.26%	87.18%	78.85%	70.83%	71.79%	60.26%
ASM	81.09%	85.58%	73.08%	74.68%	73.40%	48.08%
EMAV	84.94%	83.01%	74.68%	74.36%	75.32%	65.06%
RMS	79.17%	78.53%	72.12%	70.51%	69.23%	58.65%
STD	79.49%	80.77%	70.51%	69.55%	70.51%	59.62%
Kurt	46.47%	66.03%	42.95%	57.05%	56.41%	46.15%
SKW	43.27%	34.62%	35.26%	45.19%	44.23%	33.01%

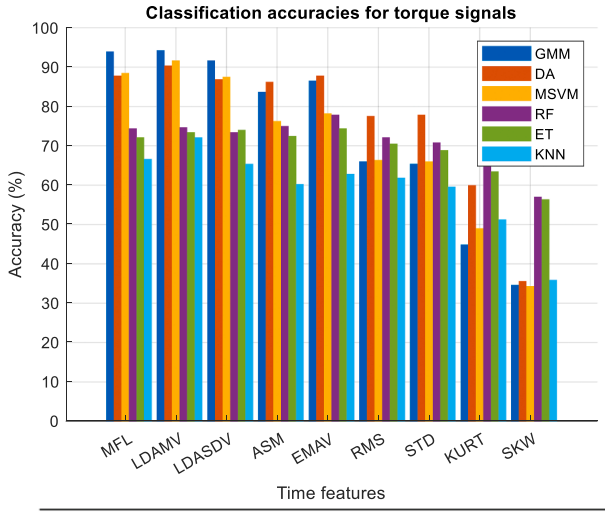

Indicators	GMM	DA	MSVM	RF	ET	KNN
MFL	93.91%	87.82%	88.46%	74.36%	72.12%	66.67%
LDAMV	94.23%	90.38%	91.67%	74.68%	73.40%	72.12%
LDASDV	91.67%	86.86%	87.50%	73.40%	74.04%	65.38%
ASM	83.65%	86.22%	76.28%	75.00%	72.44%	60.26%
EMAV	86.54%	87.82%	78.21%	77.88%	74.36%	62.82%
RMS	66.03%	77.56%	66.35%	72.12%	70.51%	61.86%
STD	65.38%	77.88%	66.03%	70.83%	68.91%	59.62%
Kurt	44.87%	59.94%	49.04%	65.06%	63.46%	51.28%
SKW	34.62%	35.58%	34.29%	57.05%	56.41%	35.90%

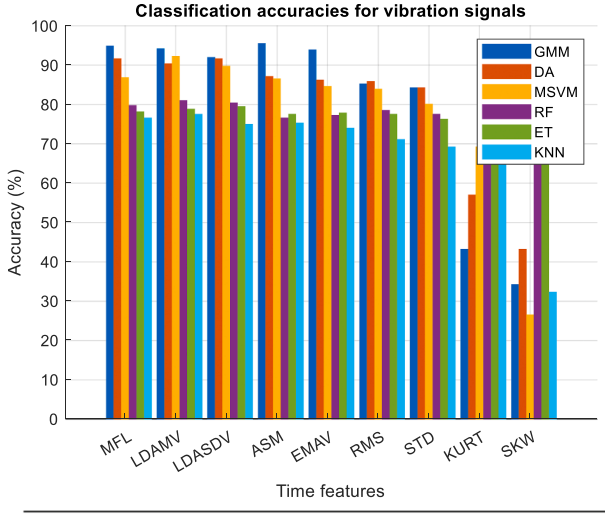

Indicators	GMM	DA	MSVM	RF	ET	KNN
MFL	94.87%	91.67%	86.86%	79.81%	78.21%	76.60%
LDAMV	94.23%	90.38%	92.31%	81.09%	78.85%	77.56%
LDASDV	91.99%	91.67%	89.74%	80.45%	79.49%	75.00%
ASM	95.51%	87.18%	86.54%	76.60%	77.56%	75.32%
EMAV	93.91%	86.22%	84.62%	77.24%	77.88%	74.04%
RMS	85.26%	85.90%	83.97%	78.53%	77.56%	71.15%
STD	84.29%	84.29%	80.13%	77.56%	76.28%	69.23%
Kurt	43.27%	57.05%	69.23%	79.49%	76.92%	79.17%
SKW	34.29%	43.27%	26.60%	64.74%	65.38%	32.37%

Fig. 17. Classification accuracies using different health indicators and classification models.

values [63].

Phase 1: Best trees group (N_1): Well-placed trees which receive sufficient food and light due to their height are considered. Older, taller, and smoother trees grow more slowly than younger ones. The competition during phase 1 focuses on nutrient acquisition, with older trees concentrating on root nutrition because of their slower growth rate

Phase 2: Light-group competition (N_2): Less light-competitive trees attempt to reposition by varying their angles to adjacent, taller, older trees, accessing light through the spaces created by these larger trees.

Phase 3: Remove and replace (N_3): The worst solutions (trees) in the population are eliminated. New candidate solutions, generated within the feasible domain of the search space, randomly replace the inferior

Algorithm 1 TGA pseudo-code

```
Initialize a pseudo-random population T, set iteration counter t=1
while t < MaxIter do
  Evaluate population and sort all solutions by fitness
  Divide population into subsets N1 and N2
  for each solution Ti in N1 do
    Perform local search using:
      Ti(j+1) = Ti(j)/ϑ + r * Ti(j), where Ti(j+1) ∈ [lb, ub]
    Apply greedy selection between old and new solution
   end for
   for each solution Ti in N2 do
    Calculate distance di to nearest best solution in N1:
       di = sqrt(Σ(T_N2^j - T_i^j)²) for j = 1 to N1 + N2
       if T_N2^j ≠ T_i^j then use computed di
       else set di = ∞
    Compute direction vector:
       y = λx₁ + (1 - λ)*x₂
       T_N2^j = T_N2^j + αi * y, where T_N2^j ∈ [lb, ub]
     Apply greedy selection between old and new solution
   end for
   Eliminate worst solutions N3 and replace with random solutions
   Generate uniformly distributed solutions N4
   Modify N4 using mix operator based on best solutions in N1
   Evaluate population and sort by fitness
   Select best N solutions for next generation
   t = t + 1
end while
return the best solution
```

Fig. 18. TGA pseudo-code [44].

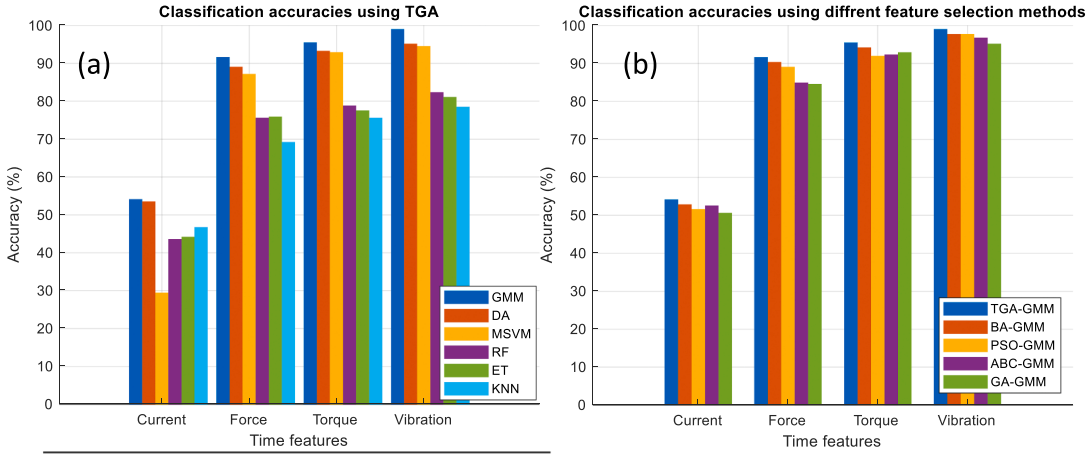

Methods	Current	Force	Torque	Vibration
TGA-GMM	54.17%	91.67%	95.51%	99.04%
TGA-DA	53.53%	89.10%	93.27%	95.19%
TGA-MSVM	29.49%	87.18%	92.95%	94.55%
TGA-RF	43.59%	75.64%	78.85%	82.37%
TGA-ET	44.23%	75.96%	77.56%	81.09%
TGA-KNN	46.79%	69.23%	75.64%	78.53%

Methods	Current	Force	Torque	Vibration
TGA-GMM	54.17%	91.67%	95.51%	99.04%
BA-GMM	52.88%	90.38%	94.23%	97.76%
PSO-GMM	51.60%	89.10%	91.99%	97.76%
ABC-GMM	52.56%	84.94%	92.31%	96.79%
GA-GMM	50.64%	84.62%	92.95%	95.19%

Fig. 19. Classification accuracies using features selected by TGA (a) and other feature selection methods (b).

ones. This process allows the worst trees to be discarded and replaced.

Phase 4: Reproduction phase (N_4): After discarding the worst trees, this phase focuses on generating new solutions. Each solution is formed by applying a mask operator to the best solution in set *N1*, which contains the best-performing individuals. Tall, good trees, benefiting from favorable conditions, begin reproducing and generating new plants. These new plants inherit certain characteristics from their mother trees, reflecting their proximity to the main tree. The algorithm's mathematical model is summarized in the TGA pseudo code in Fig. 18. With r and λ are random variables with a standard uniform distribution in [0,1], and θ is the reduction rate of tree power due to strong growth, aging and food depletion. x_1 and x_2 are selected with minimum distance di, with α_i representing a uniformly distributed angle in (0,1).

Accurate classification depends highly on features quality, particularly when processing large datasets. Reducing input variables simultaneously decreases computational cost and improves model performance. Subsection 3.4.2 and 3.4.3 combine the five proposed health indicators to improve tool condition monitoring in

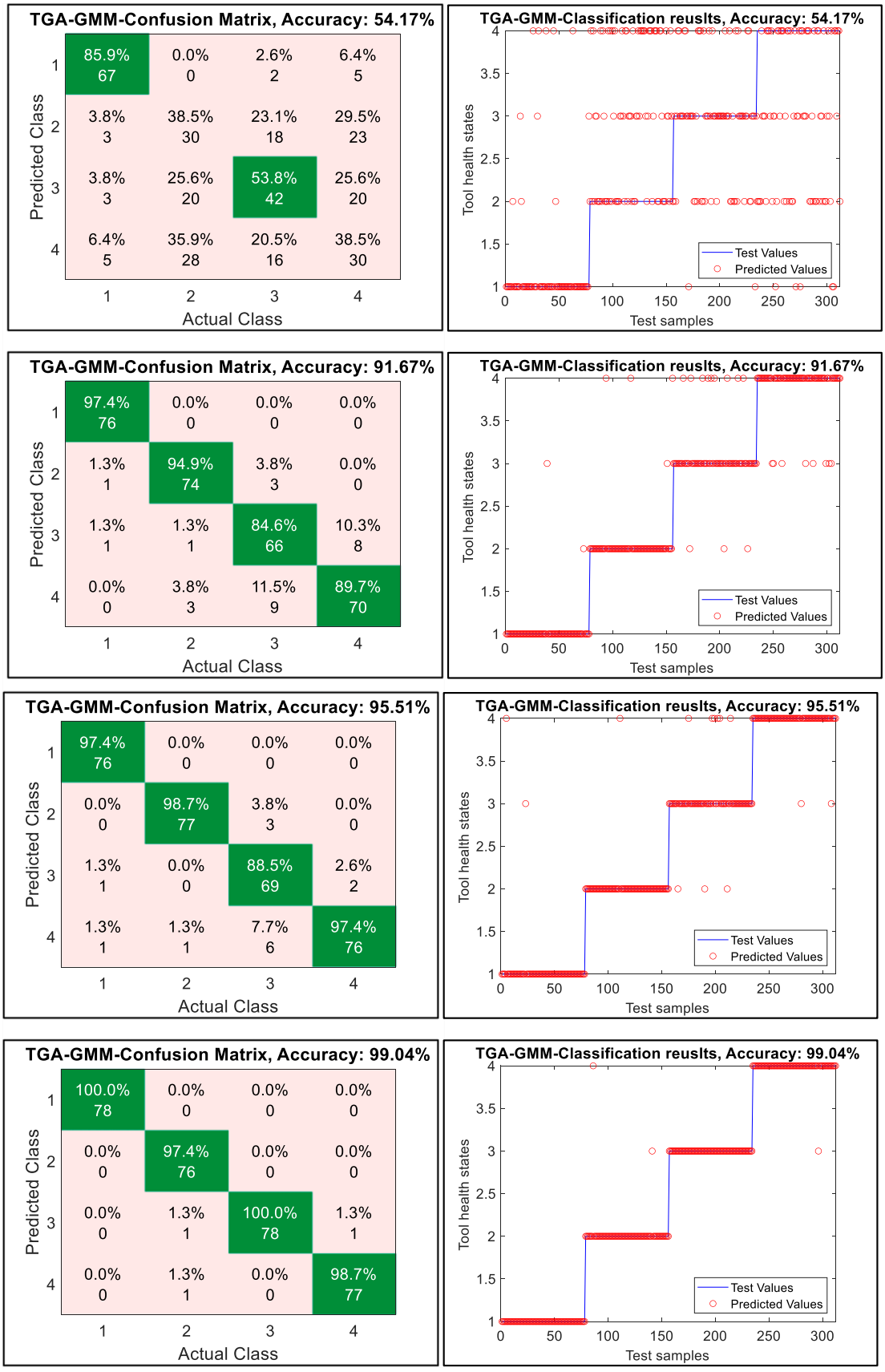

Fig. 20. TGA-GMM confusion matrix and classification results.

Table 5
Training and prediction times for different classifiers.

Classifier	Total training time (s)		Avg time per fold (s)		Avg prediction time (s)	
	No-TGA	TGA	No-TGA	TGA	No-TGA	TGA
GMM	0.1248	0.0608	0.0106	0.0052	0.0013	0.0005
DA	0.4920	0.2443	0.0441	0.0212	0.0040	0.0015
MSVM	0.3593	0.3051	0.0332	0.0281	0.0024	0.0017
RF	15.1213	11.8720	1.3198	1.0060	0.1913	0.1779
ET	3.5827	2.9360	0.3343	0.2691	0.0233	0.0226
KNN	0.1050	0.0491	0.0067	0.0021	0.0033	0.0009

Table 6
Training and testing dataset configuration.

Dataset portion	Cutting tool state			
	Healthy	Surface damage	Flake damage	Broken tooth
Training/validation (80 %)	62	62	62	62
Testing (20 %)	16	16	16	16

manufacturing systems. By using TGA for feature selection, the most relevant features are identified, while redundant and less informative ones are eliminated. This refinement enhances model generalization and predictive accuracy, thereby improving automated tool failure detection and diagnostics.

3.4.2. Tool fault classification using TGA-GMM

Each combined feature matrix obtained in subsection 3.2.2 is reduced using TGA, selecting only the most relevant features. To demonstrate TGA's suitability as a robust feature selection approach, this subsection presents a comparative analysis of TGA's performance against other feature selection methods, including bat algorithm (BA), particle swarm optimization (PSO), artificial bee colony (ABC) and genetic algorithm (GA), using the same feature sets. Fig. 19 illustrates the overall accuracies obtained by various classifiers with features selected by TGA (a) and these alternative feature selection methods (b). Fig. 20 displays the confusion matrices and classification results using TGA-GMM.

TGA has significantly increased classification accuracy by selecting highly discriminating features, particularly relevant for fault detection and diagnosis, through a phase-based structure that simulates inter-tree competition for resources. TGA provides optimized feature selection, leading to automatic classification performance improvements across all models. For instance, TGA-GMM achieves impressive accuracies of 99.04 % for vibration, 95.51 % for torque, and 91.67 % for force, while TGA-DA and TGA-MSVM also perform particularly better (Fig. 19(a)). Moreover, TGA enhances RF and ET performance relative to their performance previously (see Fig. 17), notably for vibration features, demonstrating their improved defect classification capabilities with selected features. Furthermore, in comparison with other feature selection methods (Fig. 19 (b)) using GMM as a classifier, TGA-GMM consistently achieves the highest accuracies, exceeding any other method.

To prove that our proposed approach optimally reduces computational costs, Table 5 presents training time (s), average training time per fold (s) and average prediction time (s) for each classifier trained and tested on the combined five feature matrices using vibration signals, with and without TGA for feature selection.

TGA's adaptability to complex, non-linear models enables classifiers like GMM, DA, and MSVM to achieve high accuracy while enhancing the performance of resource-intensive models such as RF and ET. TGA's phase-based structure improves both exploration and exploitation, reducing premature convergence by dynamically adjusting the search space through selective phases. As shown in Table 5, TGA reduces the running time for every classifier compared to the results without TGA, further validating its efficiency in reducing computational cost. TGA is less sensitive to parameters and highly adaptable to high-dimensional data, efficiently focusing on the most relevant features. Conversely, GA, PSO, BA, and ABC exhibit certain limitations: GA involves high computational costs due to repetitive crossover and mutation operations, PSO is prone to premature convergence in complex search spaces, and BA and ABC struggle to achieve local search accuracy. Additionally, these methods often require extensive hyperparameter tuning, increasing complexity and limits scalability.

3.4.3. Tool fault classification using TGA-GMM using unseen data

To assess the proposed technique's generalizability in tool condition classification, the selected vibration feature matrices using TGA are divided, with 80 % (62 samples) used for training and validation, and 20 % unseen data (16 samples) for testing, as illustrated in Table 6. Notably, the data are collected under variable operating conditions, demonstrating the model's generalizability by being trained under specific conditions and tested on unseen data involving other parameters such as cutting depth, spindle speed and feed rate, while providing highly accurate classification, confirming its adaptability.

GMM is cross-validated ten separate times on 80 % of the features selected by TGA, producing ten distinct classification models. Afterward, the best-performing model, based on the highest validation accuracy, is tested using the unseen data set (See Fig. 21). Fig. 22 presents the validation and test confusion matrices, along with the corresponding classification results.

The overall accuracy achieved using the selected vibration features

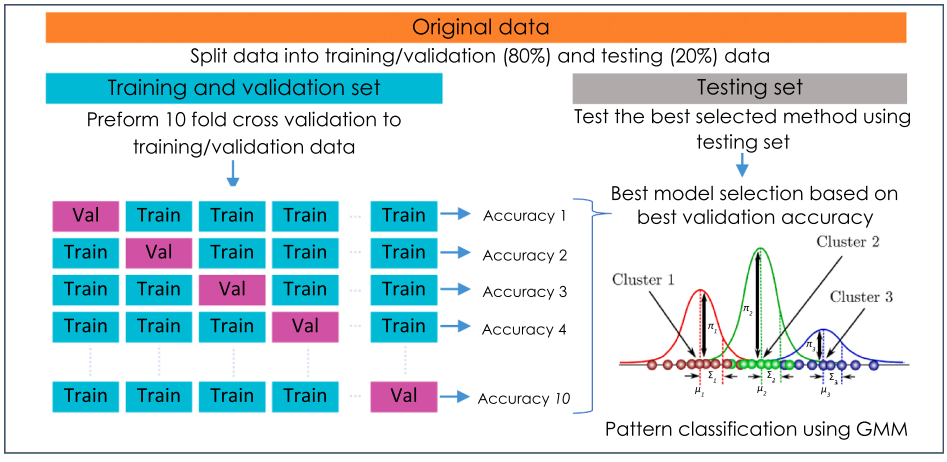

Fig. 21. Methodology for training, validation, and testing.

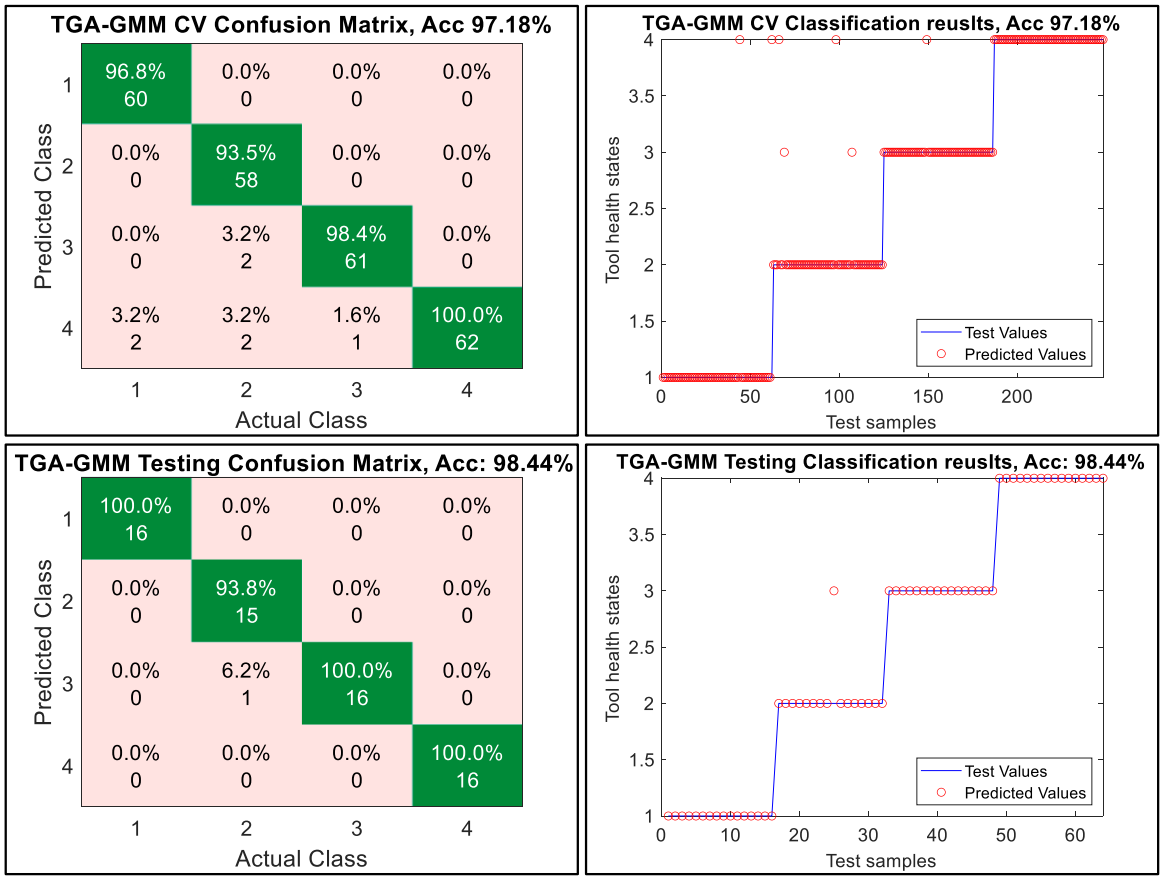

Fig. 22. TGA-GMM validation and testing confusion matrices and classification results.

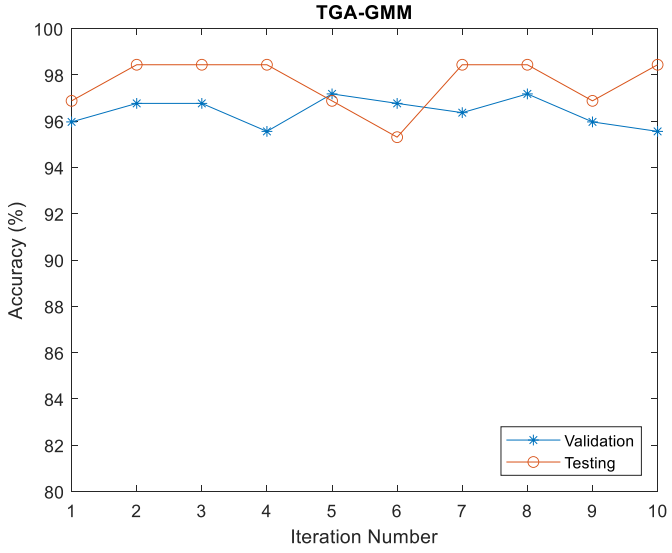

Fig. 23. Ten TGA-GMM accuracies tested with unseen vibration data.

in the validation equals 97.18 %, while the model testing accuracy on unseen data reaches 98.44 % (Fig. 22). Practically no misclassification is observed across the four classes, reinforcing the proposed approach's efficiency in classifying defects in manufacturing systems. The high classification accuracy obtained during testing demonstrates that the proposed methodology can effectively extract and select only relevant features to classify unseen data and varying operating conditions.

3.4.4. *TGA-GMM stability*

Model stability is examined in Fig. 23 by comparing the model's accuracy over ten training, validation, and testing iterations. This analysis provides valuable insights into the models' reliability and consistency in acheving accurate results. Examining model stability is fundamental to identifying potential issues related to overfitting, model sensitivity, or data variability. A remarkably accurate and stable model is produced even when tested on unseen data, resulting in highly satisfactory defect classification results and clearly demonstrating our classification method's potential.

4. Conclusion

This article highlights that advanced and reliable tool condition monitoring in manufacturing systems requires the integration of the tree growth algorithm (TGA) for feature selection with Gaussian mixture models (GMM) for feature classification. Both methodology and the entire experimental process have been described in detail, demonstrating significant improvements in classification accuracy through selecting only relevant features. The proposed methodology achieves high accuracies, 99.04 % for vibration, 95.51 % for torque, and 91.67 % for force, and proves robust generalizability and stability once tested using unseen data with 98.44 % accuracy. TGA's flexibility and efficiency in feature selection, combined with the probabilistic GMM nature, provide a superior approach to deal with complex and overlapping data distributions. Future works will involve validating the proposed framework in various manufacturing scenarios and further exploring additional feature extraction techniques to improve diagnostic capabilities. Additionally, incorporating real-time data acquisition and processing systems could facilitate the development of a more responsive tool monitoring framework, enabling timely intervention and

maintenance.

Link: https://search-data.ubfc.fr/FR-13002091000019–2023-03–06-02_METALLICADOUR-Detection-and-diagnostics-of.html

Ethical Approval

The authors did not receive support from any organization for the submitted work.

Declaration

The authors confirm that no similar paper is under review or that has already been published in another venue.

CRediT authorship contribution statement

Adel Afia: Writing – original draft. **Fawzi Gougam:** Writing – review & editing. **Abdenour Soualhi:** Validation, Supervision. **Mohammed Wadi:** Validation, Supervision. **Mohamed Tahi:** Writing – review & editing. **Mohammed Amine Sahraoui:** Writing – review & editing.

Declaration of Competing Interest

The authors declare that they have no known competing financial interests or personal relationships that could have appeared to influence the work reported in this paper.

References

1 Lee Jay, Bagheri Behrad, Kao Hung-An. A cyber-physical systems architecture for industry 4.0-based manufacturing systems. Manuf Lett 2015;3:18–23.
2 Soualhi Moncef, Nguyen Khanh TP, Medjaher Kamal. Pattern recognition method of fault diagnostics based on a new health indicator for smart manufacturing. Mech Syst Signal Process 2020;142:106680.
3 Grzesik Wit. Machining Economics and Optimization. Adv Mach Process Met Mater Theory Model Appl 2 2017:265–83.
4 Brito Lucas Costa, da Silva Márcio Bacci, Duarte Marcus Antonio Viana. Identification of cutting tool wear condition in turning using self-organizing map trained with imbalanced data. J Intell Manuf 2021;32(1):127–40.
5 Liu Meng, Takagi Jun-ichiro, Tsukuda Akira. Effect of tool nose radius and tool wear on residual stress distribution in hard turning of bearing steel. J Mater Process Technol 2004;150(3):234–41.
6 Rizal M, Ghani JA, Nuawi MZ, Haron CHC. "Cutting tool wear classification and detection using multi-sensor signals and Mahalanobis-Taguchi System. Wear 2017; 376-377:1759–65.
7 Gougam F, Soualhi M, Soualhi A, Afia A, Touzout W, Aitchikh MA. Automated fault diagnosis using maximal overlap discret wavelet packet transform and principal components analysis. PHM Soc Eur Conf 2024;8(1):7.
8 Sahraoui MA, Rahmoune C, Damou A, Gougam F, Afia A. Advancing condition-based maintenance of naval propulsion systems with ensemble learning techniques. Adv Mech Eng 2024;16(11). 16878132241298373.
9 Afia A, Soualhi M, Gougam F, Touzout W, Ait-Chikh A, Meloussi M. Enhancing gearbox condition monitoring using randomized singular value decomposition and K-nearest neighbor. PHM Soc Eur Conf 2024;8(1):7.
10 Pandit R, Astolfi D, Hong J, Infield D, Santos M. SCADA data for wind turbine data-driven condition/performance monitoring: A review on state-of-art, challenges and future trends. Wind Eng 2023;47(2):422–41.
11 Gougam F, Rahmoune C, Benazzouz D, Afia A, Zair M. Bearing faults classification under various operation modes using time domain features, singular value decomposition, and fuzzy logic system. Adv Mech Eng 2020;12(10): 1687814020967874.
12 Atamuradov Vepa, et al. Prognostics and health management for maintenance practitioners-Review, implementation and tools evaluation. Int J Progn Health Manag 2017;8(3):1–31.
13 Weiss Brian A, Qiao Guixiu. Hierarchical decomposition of a manufacturing work cell to promote monitoring, diagnostics, and prognostics. International Manufacturing Science and Engineering Conference, 50749. American Society of Mechanical Engineers; 2017.
14 D. Patange A, Jegadeeshwaran R, S. Bajaj N, N. Khairnar A, A. Gavade N. Application of machine learning for tool condition monitoring in turning. Sound 2022;Vib 56: 127–45.
15 Patange Abhishek D, Jegadeeshwaran R. Application of bayesian family classifiers for cutting tool inserts health monitoring on CNC milling. Int J Progn Health Manag 2020;11(2).
16 Bahador A, Du C, Ng HP, Dzulqarnain NA, Ho CL. Cost-effective classification of tool wear with transfer learning based on tool vibration for hard turning processes. Measurement 2022;201:111701.
17 Aralikatti SS, Ravikumar KN, Kumar H, Nayaka HS, Sugumaran V. Comparative study on tool fault diagnosis methods using vibration signals and cutting force signals by machine learning technique. Struct Durab Health Monit 2020;14(2):127.
18 Soualhi, Moncef, et al. Health indicator construction for system health assessment in smart manufacturing. prognostics and system health management conference (PHM-Paris), 2019. IEEE; 2019.
19 Olalere IO, Olanrewaju OA. Tool and workpiece condition classification using empirical mode decomposition (EMD) with Hilbert–Huang transform (HHT) of vibration signals and machine learning models. Appl Sci 2023;13(4):2248.
20 Mpoyi DK, Ekuakille AL, Ugwiri MA, Casavola C, Pappalettera G. Wear monitoring based on vibration measurement during machining: An application of FDM and EMD. Meas Sens 2024;32:101051.
21 Mutra RR, Reddy DM, Amarnath M, Rani MA, Yunus MA, Sani MSM. Artificial Neural Network-Based Fault Diagnosis of Gearbox using Empirical Mode Decomposition from Vibration Response. Int J Automot Mech Eng 2023;20(3):10695–709.
22 Kumar A, Berrouche Y, Zimroz R, Vashishtha G, Chauhan S, Gandhi CP, Xiang J. Non-parametric Ensemble Empirical Mode Decomposition for extracting weak features to identify bearing defects. Measurement 2023;211:112615.
23 Afia Adel, et al. Gearbox fault diagnosis using REMD, EO and machine learning classifiers. J Vib Eng Technol 2024;12(3):4673–97.
24 Sun L, Zhao C, Huang X, Ding P, Li Y. Cutting tool remaining useful life prediction based on robust empirical mode decomposition and Capsule-BiLSTM network. Proceedings Institution Mechanical Engineers Part C Journal Mechanical Engineering Science 2023;237(14):3308–23.
25 Goyal D, Choudhary A, Sandhu JK, Srivastava P, Saxena KK. An intelligent self-adaptive bearing fault diagnosis approach based on improved local mean decomposition. Int J Interact Des Manuf (IJIDeM) 2022:1–11.
26 Yuan J, Liu L, Yang Z, Zhang Y. Tool wear condition monitoring by combining variational mode decomposition and ensemble learning. Sens (Basel Switz) 2020;20 (21):6113.
27 Wei W, He G, Yang J, Li G, Ding S. Tool wear monitoring based on the gray wolf optimized variational mode decomposition algorithm and Hilbert–Huang transformation in machining stainless steel. Machines 2023;11(8):806.
28 Liu Z, Peng D, Zuo MJ, Xia J, Qin Y. Improved Hilbert–Huang transform with soft sifting stopping criterion and its application to fault diagnosis of wheelset bearings. ISA Trans 2022;125:426–44.
29 Tahi M, Miloudi A, Afia A. Fault diagnosis in gearbox system with MODWT and MODWPT using SVM and RF algorithms. J Test Eval 2025;53(4).
30 Jelila YD, Pamuła W. Application of MEMS sensors for the condition monitoring of urban tramways based on MODWPT. IEEE Sens J 2023;23(20):24300–7.
31 Yao R, Jiang H, Yang C, Zhu H, Liu C. An integrated framework via key-spectrum entropy and statistical properties for bearing dynamic health monitoring and performance degradation assessment. Mech Syst Signal Process 2023;187:109955.
32 Afia A, Gougam F, Rahmoune C, Touzout W, Ouelmokhtar H, Benazzouz D. Intelligent fault classification of air compressors using Harris hawks optimization and machine learning algorithms. Trans Inst Meas Control 2024;46(2):359–78.
33 Yongdong S, Junxian S, Yonggang L. Early weak fault signal enhancement and recognition method of rudder paddle bearings based on parameter adaptive stochastic resonance. IEEE Access 2023.
34 Damou A, Ratni A, Benazzouz D. Intelligent multi-fault identification and classification of defective bearings in gearbox. Adv Mech Eng 2024;16(4): 16878132241246673.
35 Adel A, Hand O, Fawzi G, Walid T, Chemseddine R, Djamel B. Gear fault detection, identification and classification using MLP neural network. In Recent Advances in Structural Health Monitoring and Engineering Structures: Select Proceedings of SHM and ES 2022. Singapore: Springer Nature Singapore; 2022. p. 221–34.
36 Gougam F, Afia A, Aitchikh MA, Touzout W, Rahmoune C, Benazzouz D. Computer numerical control machine tool wear monitoring through a data-driven approach. Adv Mech Eng 2024;16(2):16878132241229314.
37 Touzout W, Benazzouz D, Gougam F, Afia A, Rahmoune C. Hybridization of time synchronous averaging, singular value decomposition, and adaptive neuro fuzzy inference system for multi-fault bearing diagnosis. Adv Mech Eng 2020;12(12): 1687814020980569.
38 Chen K, Xue B, Zhang M, Zhou F. An evolutionary multitasking-based feature selection method for high-dimensional classification. IEEE Trans Cybern 2020;52(7): 7172–86.
39 Tran Minh-Quang, Liu Meng-Kun, Tran Quoc-Viet. Milling chatter detection using scalogram and deep convolutional neural network. Int J Adv Manuf Technol 2020; 107(3):1505–16.
40 Al-Tashi Q, Abdulkadir SJ, Rais HM, Mirjalili S, Alhussian H. Approaches to multi-objective feature selection: a systematic literature review. IEEE Access 2020;8: 125076–96.
41 Bommert Andrea, et al. Benchmark for filter methods for feature selection in high-dimensional classification data. Comput Stat Data Anal 2020;143:106839.
42 Gao Yuanyuan, Zhou Yongquan, Luo Qifang. An efficient binary equilibrium optimizer algorithm for feature selection. IEEE Access 2020;8:140936–63.
43 Al-Saffar, Suzan Muhsen, and Omar S.Qasim. Enhanced Binary Tree Growth Algorithm with Linear Discriminant Analysis for Leukemia Dataset Classification.
44 Cheraghalipour Armin, Hajiaghaei-Keshteli M. Tree growth algorithm (TGA): An effective metaheuristic algorithm inspired by trees behavior.". 13th International Conference on Industrial Engineering, 13; 2017.
45 Singh Ratima Raj, Vijh Surbhi, Chaubey Diwakar. An efficient brain tumor detection using modified tree growth algorithm and random forest method. Sixth International Conference on Image Information Processing (ICIIP), 6. IEEE; 2021. 2021.

46 Too J, Abdullah AR, Mohd Saad N, Mohd Ali N. Feature selection based on binary tree growth algorithm for the classification of myoelectric signals. Machines 2018;6 (4):65.
47 Gougam F, Afia A, Soualhi A, Touzout W, Rahmoune C, Benazzouz D. Bearing faults classification using a new approach of signal processing combined with machine learning algorithms. J Braz Soc Mech Sci Eng 2024;46(2):65.
48 Soualhi M, Soualhi A, Nguyen T-P, Medjaher K, Clerc G, Razik H. LASPI: Détection et diagnostic des défauts de boîte de vitesses. LASPI 2023. https://doi.org/10.25666/DATAUBFC-2023-03-06.
49 Jablonski A, Barszcz T, Bielecka M, Breuhaus P. Modeling of probability distribution functions for automatic threshold calculation in condition monitoring systems. Measurement 2013;46(1):727–38.
50 Bishop Christopher M, Nasser MNasrabadi. Pattern recognition and machine learning, 4. New York: springer; 2006.
51 Panić Branislav, Jernej Klemenc, Marko Nagode. Gaussian Mixture Model Based Classification Revisited: Application to the Bearing Fault Classification. Strojški Vestn J Mech Eng 2020;66:215–26.
52 Haghani Adel, Jeinsch Torsten, Ding Steven X. Quality-related fault detection in industrial multimode dynamic processes. IEEE Trans Ind Electron 2014;61(11): 6446–53.
53 Ni L, Wang D, Wu J, Wang Y, Tao Y, Zhang J, Liu J. Streamflow forecasting using extreme gradient boosting model coupled with Gaussian mixture model. J Hydrol 2020;586:124901.
54 Zhuangzhuang Zhu, Zhiping Zhou. "Gaussian mixture generative model to detect abnormal health data. Comput Sci Explor 2021;1.
55 Cao S, Hu Z, Luo X, Wang H. Research on fault diagnosis technology of centrifugal pump blade crack based on PCA and GMM. Measurement 2021;173:108558.
56 Zhang B, Yan X, Liu G, Fan K. Multi-source fault diagnosis of chiller plant sensors based on an improved ensemble empirical mode decomposition Gaussian mixture model. Energy Rep 2022;8:2831–42.
57 Zhang J, Yan J, Infield D, Liu Y, Lien F. Short-term forecasting and uncertainty analysis of wind turbine power based on long short-term memory network and Gaussian mixture model. Appl Energy 2019;241:229–44.
58 Glowacz A, Glowacz W, Glowacz Z, Kozik J. Early fault diagnosis of bearing and stator faults of the single-phase induction motor using acoustic signals. Measurement 2018;113:1–9.
59 Soualhi M, Soualhi A, Nguyen KTP, Medjaher K, Guy C, Hubert R. Open heterogeneous data for condition monitoring of multi faults in rotating machines used in different operating conditions. Int J Progn Health Manag 2023;14(2).
60 Shan Pei-Wei, Li Ming. Nonlinear time-varying spectral analysis: HHT and MODWPT. Math Probl Eng 2010;2010.
61 Reynolds D. Gaussian Mixture Models. In: Li SZ, Jain A, editors. Encyclopedia of Biometrics. Boston, MA: Springer; 2009. https://doi.org/10.1007/978-0-387-73003-5_196.
62 Strumberger Ivana, et al. Dynamic search tree growth algorithm for global optimization. Proceedings 10. Technological Innovation for Industry and Service Systems: 10th IFIP WG 5.5/SOCOLNET Advanced Doctoral Conference on Computing, Electrical and Industrial Systems. Costa de Caparica, Portugal: Springer International Publishing; 2019. p. 2019. Proceedings 10.
63 Strumberger I, Minovic M, Tuba M, Bacanin N. Performance of elephant herding optimization and tree growth algorithm adapted for node localization in wireless sensor networks. Sens (Basel Switz) 2019;19(11):2515.